Published in final edited form as:
Phys Med Biol. 2011 March 21; 56(6): 1755–1773. doi:10.1088/0031-9155/56/6/015.

Comparison of Blood Velocity Measurements between Ultrasound Doppler and Accelerated Phase-Contrast MR Angiography in Small Arteries with Disturbed Flow

Jingfeng Jiang[1], **Charles Strother**[2], **Kevin Johnson**[1], **Sara Baker**[3], **Dan Consigny**[2], **Oliver Wieben**[1,2], and **James Zagzebski**[1,2,3]

[1]Medical Physics Department, University of Wisconsin-Madison, School of Medicine and Public Health

[2]Radiology Department, University of Wisconsin-Madison, School of Medicine and Public Health

[3]School of Ultrasound, University of Wisconsin-Madison, School of Medicine and Public Health

Abstract

Ultrasound Doppler (UD) velocity measurements are commonly used to quantify blood flow velocities *in vivo*. The aim of our work was to investigate the accuracy of *in vivo* spectral Doppler measurements of velocity waveforms. Waveforms were derived from spectral Doppler signals and corrected for intrinsic spectral broadening errors by applying a previously published algorithm. The method was tested in a canine aneurysm model by determining velocities in small arteries (3-4 mm diameter) near the aneurysm where there was moderately disturbed flow. Doppler results were compared to velocity measurements in the same arteries acquired with a rapid volumetric phase contrast MR Angiography technique named PC-VIPR MRA. After correcting for intrinsic spectral broadening, there was a high degree of correlation between velocities obtained by the real-time UD and the accelerated PC-MRA technique. The peak systolic velocity yielded a linear correlation coefficient of $r = 0.83$; end diastolic velocity resulted in $r = 0.81$; and temporally-averaged mean velocity resulted in $r = 0.76$. The overall velocity waveforms obtained by the two techniques were also highly correlated ($r = 0.89 \pm 0.06$). There were, however, only weak correlations for the pulsatility index (PI; 0.25) and resistive index (RI; 0.14) derived from the two techniques. Results demonstrate that to avoid overestimations of peak systolic velocities, the results for UD must be carefully corrected to compensate for errors caused by intrinsic spectral broadening.

Keywords

Ultrasound Doppler; Phase-contrast Magnetic Resonance Angiography; Aneurysm; Computational Fluid Dynamics

1. Introduction

The etiology and progression of many cardiovascular abnormalities are associated with certain patterns of blood flow. Consequently, blood flow imaging is of clinical interest because it provides insight into factors that relate both to the progression of these disorders and to changes in flow that occur following their treatment. Ultrasound Doppler [UD]

Address correspondence to: Jingfeng Jiang, PhD, Department of Medical Physics, WIMR-1005, 1111 Highland Ave., Madison, WI 53705, The University of Wisconsin-Madison, Madison, WI-53706, USA., **Voice:** (608)-262-4197, **Fax:** (608)-262-2413, jjiang2@wisc.edu.

velocity measurements are a noninvasive and cost-effective method to provide blood velocity information (Gill, 1985; Hoskins, 1990). In addition to blood velocities, other parameters e.g. pressure gradients (Holen *et al.*, 1987; Faccenda *et al.*, 1990) and wall shear stress [WSS] (Hughes and How, 1993) have been quantified using UD Velocity measurements. For instance, the pressure gradient, a clinically-relevant parameter for the assessment of the severity of an arterial stenosis (Gross *et al.*, 2001) is typically calculated by applying the modified Bernoulli equation (Fuster, 2008). It is thus important to understand the sources of potential error in Doppler velocity measurements and to make any necessary corrections that will assure accuracy of results.

Early work using simple flow phantoms demonstrated the potential for UD velocity assessments performed on spectral displays to overestimate blood velocities, largely because of intrinsic spectral broadening (ISB) (Hoskins, 1996; Eicke *et al.*, 1995). Several small scale clinical or preclinical animal studies (Lee *et al.*, 1997; Stadlbauer *et al.*, 2009; Wendt *et al.*, 1992; Hoppe *et al.*, 1998; Seitz *et al.*, 2001a, 2001b) have also compared UD velocity measurements to those obtained using 2D phase-contrast magnetic resonance (PC-MR) angiography. In these comparisons, typically peak systolic velocities measured by UD were higher than velocities measured using PC-MR, and correlation coefficients between the two measurements ranged from 0.328 to 0.96 (Lee *et al.*, 1997; Stadlbauer *et al.*, 2009; Wendt *et al.*, 1992; Hoppe *et al.*, 1998; Seitz *et al.*, 2001a, 2001b).

It is recommended that clinical UD velocity measurements be performed at Doppler angles less than 60° to minimize such overestimation (Allan, 2006). In the case where the long axis of a vessel lies parallel to the skin surface (*e.g.* as for the common carotid artery), using a small Doppler angle may, however, not be feasible due to limited beam steering angles available with most ultrasound transducers. Also, to our knowledge, little attention has been paid to the manner in which the Doppler spectral velocity display should be interpreted so as to minimize errors caused by the intrinsic spectral broadening effect. One objective of this study was to develop a practical tracing method that could improve accuracy and reproducibility of UD velocity measurements when the Doppler angle was relatively large (Doppler angle of 40-70 degrees). Our second goal was to expand the quantitative comparisons of velocity measurements by UD and PC-MR techniques for moderately disturbed blood flow in small arteries (3-4 mm diameter). Specifically, blood velocity waveforms measured by UD after corrections were compared with those obtained using PC-VIPR (Gu *et al.*, 2005), an accelerated volumetric PC-MRA technique with three directional flow encoding. Measurements were performed in and around experimental canine aneurysms in a region of disturbed flow (Turk *et al.*, 2007). The presence of one or more aneurysms (acting as a cavity or cavities) leads to flow disturbance in and around the aneurysm\s. In other words, locally disturbed laminar flow is often observed in and around aneurysms located at small (3-4 mm diameter) arteries at physiological Reynold's numbers (*e.g.* 100-500), but no signs of fully developed turbulence have been reported (Steiger *et al.*, 1987). On the one hand, disturbed flow adds additional spectral broadening effects in the UD velocity measurements (Douville *et al.*, 1985). On the other hand, since PC-VIPR MRA measurements assume a uniform velocity distribution within the resolution cell, disturbed flow leads to intra-voxel dephasing, where spins within the resolution cell become randomly oriented such that the accuracy of velocity measurements is significantly affected (Dyverfeldt *et al.*, 2008).

Because of the presence of disturbed flow, velocity measurements obtained with either technique are subject to errors. To help in understanding the extent and causes of disagreements between results from the two imaging approaches, we have also included computer simulated velocity values obtained using classic, animal-specific (*i.e.* image-based geometries and pulsatile flow waves adjacent to the regions of interest) computational fluid

dynamics (CFD) simulations (Steinman *et al.*, 2003). Computed flows in these vessels were used to arbitrate cases where the UD and the PC-MRA velocity measurements differed significantly.

2. Materials and Methods

2.1 Selection of Subjects

Under an institutionally approved animal protocol, either a single bifurcation aneurysm or a bifurcation aneurism and a side-wall (lateral) aneurysm (Figure 1) were created in adult female Beagles using a technique originally described by German and Black (German and Black, 1965) and later modified in our laboratory (Strother *et al.*, 1992). At least three weeks after the aneurysm was produced, animals were anesthetized and then subjected to PC-VIPR MRA and Ultrasound imaging studies. In an internal database, we identified 4 animals who had the imaging procedures conducted on the same day; it was also noted that, for the same animal, there were no significant differences (< 15% difference) in the heart rates of these animals at the time of the UD and the PC-VIPR MRA examinations. Small differences in animals' heart rates ensure that PC-VIPR MRA and UD exams were performed under similar physiological conditions. Otherwise, significant changes in heart rates result in significant changes of blood velocity in the common carotid artery (Jiang *et al.*, 1995), thereby making quantitative velocity comparison among the UD and PC-VIPR more difficult. In these 4 animals, two had bifurcation aneurysms, while the other two had both a bifurcation and a side-wall aneurysm. Hereafter we refer to these four animals as Subjects A – D.

2.2 Description of the Ultrasound Doppler Examinations

The same experienced ultrasound technologist (SB) scanned all 4 animals. UD evaluations were performed using a Siemens Antares scanner (Siemens Healthcare [USA] Inc., Mountain View, CA) equipped with a 5-to-13 MHz linear array transducer (VFX13-5). The hand-held probe was positioned first over the common carotid artery (CCA; see Fig. 1) in the lower part of the neck. By moving the probe toward the bifurcation aneurysm, the examiner was able to image at least three planes related to the aneurysm (one proximal to the aneurysm that included the parent artery upstream from the aneurysm, and two distal to the aneurysm, one including the branch of the parent artery on the left side of the aneurysm and the other including the branch of the parent artery on the right side of the aneurysm). (Fig. 1) If a side-wall aneurysm was present, one additional plane distal to the side-wall aneurysm was also imaged.

The vessels were scanned in both transverse and longitudinal planes to assess the overall flow and aneurysm anatomy. Using color-flow B-mode real-time imaging as a map (see Fig. 2a), the examiner placed the pulsed Doppler sample volume (axial gate size of 2-mm) in the stream of flow in the center of the artery (approximately 4-mm diameter for a canine CCA) being examined. The corresponding focal lateral and elevational beam widths (−6 dB) are approximately 1 mm and 1.5 mm, respectively, for imaging conditions investigated (a transmit focal depth of 10~20 mm and a center frequency of 6-8 MHz). The angle correct cursor was manually aligned parallel to the flow direction. Doppler angles were approximately 60 degrees (54.4 ± 9.7 degrees; mean ± standard deviation). Obtaining angles at the 60 degree range is challenging because the vessels (10-15 mm away from the skin surface) lie approximately parallel to the skin surface. Instrument imaging adjustments (*e.g.* persistence, image depth, and transmit power) were set at fixed values. Other settings including the pulse repetition frequency and gain, however, were adjusted according to individual animals (based mainly on the peak systolic velocity and Doppler signal strength)

to obtain optimal visualization of the aneurysm anatomy and flow patterns. The UD data acquisitions were not Electrocardiogram (ECG)-gated.

2.3 Description and Calibration of the Accelerated PC-VIPR MRA Technique

MR imaging was conducted on a 1.5 T clinical scanner (Signa HD, GE Healthcare, Waukesha, WI, USA) with a standard 8-channel knee coil. The 3D PC-VIPR (Phase Contrast Vastly Undersampled Isotropic Projection Reconstruction) technique (Gu *et al.*, 2005) uses a highly accelerated 3D radial acquisition that provides isotropic voxel dimensions. PC-VIPR MRA exploits the sparsity of the phase contrast data sets and allows for high resolution imaging in relatively short acquisition windows (Gu *et al.*, 2005; Johnson *et al.*, 2008). PC-VIPR data were acquired covering the vasculature of interest using the following parameters: TE/TR of 3.6/14.0 ms, retrospective ECG gating, a bandwidth of ±31.25 kHz, a FOV of approximately 18× 18× 18 cm^3, isotropic acquired spatial resolution of 0.8 mm, and scan time of 8 minutes. Temporal resolution varies from 33 to 45 ms. For each animal a conventional 2D cine PC-MRA sequence with a high encoding velocity was first prescribed. This was subsequently used to determine the appropriate velocity encoding (Venc) for the PC VIPR acquisition, which ranged from ±1.5-2m/s. All MR experiments were conducted by MR physicists experienced in cardiovascular MRI (K. J. or O. W.).

The most-recent experimental validation of the accuracy of the PC-VIPR MRA technique was described by Nett and colleagues(Nett *et al.*, 2009) who used a MR compatible flow pump (CompuFlow 1000 MR, Shelley Medical Imaging Technologies, London, ON, Canada) and a flow phantom consisting of a 7.94 mm diameter tube filled with a blood-mimicking fluid (BMF-MR, Shelley Medical Imaging Technologies). In their study, the steady flow rates estimated with a Venc of 120 cm/s were, on average, only 0.4% less than the actual pump flow rate.

2.4 Off-line Visualization and Data Analysis

Doppler velocity spectrograms were transferred from the Antares scanner to a computer workstation (Dell Precision 390, Dell Inc., Austin, TX) for processing. A digitizer software (Engauge Digitizer, sourceforge.net) was used to measure Doppler waveforms by a single user (JJ). As shown in Fig. 2a, both the inner and outer envelopes of the spectral display were measured from all Doppler signal spectrograms. Velocity measurements on spectrograms were corrected for the intrinsic spectral broadening (ISB) effect as follows,

$$V_{corr}=\max\left(V_{outer}-\frac{V_{outer}}{\alpha},\frac{V_{outer}+V_{inner}}{2}\right) \quad (1)$$

where V_{corr} is the velocity value after correction, max(*A, B*) is the larger value of A and B and, V_{outer} and V_{inner} are velocity measurements corresponding to the outer and inner envelopes (see Fig. 2a), respectively. α is a correction factor based on theoretical derivations given by Newhouse et al (Newhouse *et al.*, 1987; Newhouse *et al.*, 1994). For completeness, a brief derivation of Eqn. (1) can be found in Appendix A .

MR-measured 4D velocity data were exported to the same computer workstation for analysis. A MATLAB (Mathworks Inc., Natick, MA) graphical user interface (GUI) (Nett *et al.*, 2009) was developed to process the time-resolved, volumetric PC-VIPR data containing three-directional velocity information. The user interface allows for the interactive placement of an oblique plane (see Fig. 2b) through the measurement volume, usually placed perpendicular to the long axis of the artery of interest. To ensure the analysis plane was perpendicular to the long axis of the artery, the algorithm first connected centroids of adjacent vessel slices to approximate the long axis and then rotated the plane until it was perpendicular to the long axis. This approach has proven to work well given straight arterial

segments like ours as shown in Fig. 2. The through plane velocity component is then calculated from the velocity vectors. The maximum through-plane velocity measurement for the given plane at each point of a cardiac cycle was used to generate V_{MRA}, the axial velocity waveform for that plane.

To ensure that velocity waveforms under the PC-VIPR MRA and UD methods were obtained from the same (at least closely adjacent) locations, we first selected an identifiable anatomical feature (*e.g.* the apex of the bifurcation aneurysm in Figs. 2a and 2b) and then manually aligned the cross-sectional plane described above to be approximately an equal distance from the anatomical feature for each modality.

The peak systolic velocity (PSV), mean velocity (MV), end diastolic velocity (EDV), pulsatility index $\left(PI=\frac{V_{PSV}-V_{EDV}}{V_{MV}}\right)$ and resistive index $\left(RI=\frac{V_{PSV}-V_{EDV}}{V_{PSV}}\right)$ determined with the UD and the PC-VIPR MRA methods were compared by the Bland-Altman Plot method (Bland and Altman, 1986). Bi-variate linear regression analyses and Spearman's linear correlations were also performed to determine correlation coefficients (r) and regression parameters (slope and intercept with the y-axis) for these five velocity parameters (PSV, MV, EDV, PI and RI) for the UD and the PC-VIPR MRA experiments. Exact permutation distributions were used to calculate P values in Matlab (Mathworks Inc., Natick, MA). A probability value of 0.05 was considered significant. Absolute differences (cm/s) were also calculated for above-mentioned five velocity parameters.

Pearson's linear correlations as well as the root mean squared errors (RMSE) were also assessed between overall velocity waveforms from both UD and the PC-VIPR MRA techniques. The RMSEs were also normalized by corresponding (temporal) mean velocity values to obtain normalized (unit-less) RMSEs.

All above-mentioned parameters obtained by applying the proposed ISB-correction method (*i.e.* Eqn. (1); hereafter referred as to the "post-correction method") are compared to the conventional tracing method (*i.e.* velocity measurements corresponding to the outer envelop of Doppler Spectral display [see Fig. 2a] and hereafter referred as to the "pre-correction method").

2.5 Description of "Animal-specific" Computational Fluid Dynamics (CFD) Simulations

3D-digital subtraction angiography (DSA) data were obtained for subject D with a bi-plane flat detector C-arm fluoroscopy system (Axiom Artis dBA, Siemens Medical System Inc., Forchheim, Germany). Images were acquired following the injection of contrast agent. A Siemens Leonardo workstation was used to convert the 3D angiographic data into a sequence of standard DICOM images. Image segmentation was done with a commercially available package named ScanIP (Simpleware Inc., Exeter, United Kingdom) to obtain realistic vessel geometries. Then, the reconstructed geometry was imported to a mesh generator ScanFE (Simpleware) to create an 3D unstructured mesh.

To compute velocity waveforms in and around the aneurism, we solved the time-dependent 3D Navier-Stokes equations [*i.e.* Eqns. (2) and (3)] for the 3D meshed vessel geometry using Fluent software, a commercially-available computational fluid dynamic (CFD) solver (version 12.0; ANSYS-FLUENT Inc., Lebanon, NH). The equations for velocity are written as:

$$\vec{\nabla} \bullet \vec{u} = 0 \qquad (2)$$

$$\rho\frac{\partial\vec{u}}{\partial t}+\rho\left(\vec{u}\bullet\vec{\nabla}\right)\vec{u}=-\vec{\nabla}p+\mu\nabla^2\vec{u} \quad (3)$$

where $\vec{u}$ is the three-dimensional velocity vector, ρ is the blood density, p is the pressure and μ is the viscosity. Blood was modeled as an incompressible laminar fluid with a density of 1050 kg/m^3 and a dynamic viscosity of 0.0035 kg/m-s. For the simulations, time step was fixed at 0.0002 seconds per step (approximately 2000 steps per cardiac cycle for subject D). For Subject D, approximately 600,000 tetrahedral cells were used to solve the Navier-Stokes equations.

The first inlet flow rate waveform needed as a part of the boundary conditions was chosen from PC-MRA measurements made upstream (approximately 4 cm; hereafter referred as to section 0) from the bifurcation aneurysm of the subject being investigated. Time-dependent flow rates were obtained by integrating the through-plane PC-MRA velocity component over the artery lumen on a slice perpendicular to the axis of the artery. It is reported that uncertainties of *in vivo* conventional PC-MRA in terms of flow rate range from 3-13% (Maguire *et al.*, 2006; Evans *et al.*, 1993; Lotz *et al.*, 2002). This accuracy remains adequate for use in establishing boundary conditions for CFD calculations (Kohler *et al.*, 2001). Since the flow rate information from UD was not available, the second inlet flow rate waveform mimicking the UD velocity waveform measured also at the section 0 of the same subject was derived by matching its peak systolic flow rate with the peak systolic flow rate of the first MRA inlet flow rate waveform.

Using inlet flow rate waveforms described above, fully developed velocities were prescribed at the inlet by weighting Womersley's analytic solution for fully developed pulsatile flow with the Fourier coefficients (Frayne *et al.*, 1995). We also assumed zero pressure outlets, resulting in a flow volume division rate of approximately 50:50 between two outlets for Subject D, which was consistent with MRA measurements.

We assumed a "no slip" boundary condition on the arterial wall (*i.e.*, velocity is zero at the wall), and walls were assumed to be rigid. The rigid wall assumption may be a limiting factor for detailed hemodynamic analysis of secondary flows (Jin *et al.*, 2003) but should be acceptable for predicting transient axial velocity waveforms along relatively straight arterial segments like ours (Rayz *et al.*, 2008). Convergence criteria for continuity (*i.e.* residual of the continuity equation) and velocity were both set to 10^{-4}. Sensitivity tests on mesh size, step size and convergence criteria in terms of simulated velocity values at selected locations were performed similar to methods described by Valencia et al. (Valencia *et al.*, 2006).

We computed flow over a total of three cardiac cycles by solving Eqns. (2) and (3); almost no differences (*i.e.* full periodicity) were observed after the second cycle. Since a steady state computation was used by Ansys Fluent 12.0 as the initial guess for the transient simulation, multiple cardiac cycles were necessary for the result to be considered as fully periodic in time. Therefore, results corresponding to the last cycle simulated will be reported below. More details using about the procedures of "image-based" CFD simulations can be found in our previous publication (Jiang and Strother, 2009).

3. Results

3.1 Comparison of Velocity Waveforms between UD and PC-VIPR

To compare the velocity waveforms obtained with the UD and the PC-VIPR MRA techniques, three or four axial sections were analyzed for each animal [see Fig. 3]; Section 1 was proximal (upstream) to the bifurcation aneurysm, Sections 2 and 3 were distal

(downstream) to the bifurcation aneurysm (across the branch to the left and right sides of the bifurcation aneurysm, respectively, when it was viewed from the front). In the two animals with a side-wall aneurysm, velocity was also measured at a plane distal (downstream) to the side-wall aneurysm (Section 4).

To evaluate correlation between velocity information obtained by the two modalities, high resolution UD velocity waveforms were re-sampled to the temporal resolution of MRA velocity measurements. Following this, the Pearson's linear correlation was computed for V_{UD} [from both the "pre-" and "post-correction" Doppler spectral data] and V_{MRA} [from MRA data] from the same site. We found high correlations for both the pre- and post-correction UD data, ranging from 0.78 to 0.98 [mean ± standard deviation: 0.89 ± 0.06 (pre) vs. 0.89 ± 0.06 (post)] between the velocity waveforms measured by PC-VIPR MRA and UD.

"Post-correction" UD and MRA velocity waveforms are displayed in Fig. 3 for all four subjects. It is easy to see, from these RMSEs including normalized RMSEs (Table 1), that differences between the UD and the MRA velocity waveforms are significant. Furthermore, the proposed correction method did not significantly improve registration between the UD and the MRA velocity waveforms, as evident by virtually unchanged normalized RMSEs [0.47 ± 0.13 (pre) vs. 0.45 ± 0.20 (post)] and RMSEs [20.5 ± 14.7 cm/s (pre) vs. 18.4 ± 10.5 cm/s (post)].

We also compared the EDV, temporally-averaged mean velocity (MV), PSV, PI and RI between the UD and PC-VIPR MRA techniques. Table 2 summarizes results for these five parameters (PSV, MV, EDV, PI and RI) of absolute difference, Bland-Altman analyses (mean difference, lower and upper limits), Spearman's correlations including *P*-values and Bivariate linear regression analyses (slope and interception with y-axes). Among PSV, MV and EDV measured by the UD and the PC-VIPR MRA methods, we found significant correlations (0.76-0.83, $p<0.005$ for the post-correction UD data and 0.78-0.85, $p<0.005$ for the pre-correction UD data). However, there were weak correlations (0.25 and 0.14 for the post-correction UD data and, 0.35 and 0.23 for the pre-correction UD data) between the PI and RI for the UD and the PC-VIPR MRA methods.

Also as shown in Table 2, as compared to the PC-VIPR MRA technique by the Bland-Altman method (see Table 2), the post-correction UD data slightly underestimated the MV and the EDV by 6.9 cm/s and 4.4 cm/s, respectively, whereas it slightly overestimated the PSV by approximately 2.6 cm/s. However, as compared to the PC-VIPR MRA technique, the pre-correction UD data significantly overestimated the PSV by approximately 29.2 cm/s (see Table 2). Also seen from Table 2, due to variations (see absolute difference values in Table 2) among measured PSVs, EDVs and MVs, UD velocity results for the PI and the RI presented relatively large discrepancies from values derived using the PC-VIPR MRA method. This is consistent with results shown in Table 1 where the normalized RMSE values indicated that large quantitative differences between the UD and PC-VIPR MRA measurements exist.

3.2 Comparison Between the "pre-" and "post-correction" UD Velocity Waveforms

We also compared the EDV, MV, PSV, PI and RI between the pre- and post-correction UD velocity parameters. Table 3 summarizes results for these five parameters (PSV, MV, EDV, PI and RI) of absolute mean difference, Bland-Altman analyses (mean difference, lower and upper limits), Spearman's correlations including *P*-values and Bivariate linear regression analyses (slope and interception with y-axes).

As compared to the post-correction UD velocity data, the pre-correction UD velocity data significantly overestimated (see the mean differences by the Bland-Altman method Table 3) all three parameters (PSV, MV EDV) by 26.6 cm/s (or 29.0%), 13.4 cm/s (or 28.2%) and 7.2 cm/s (or 25.2%), respectively. It is interesting to note that the mean absolute differences are equal to the mean differences among PSV, MV and EDV in Table 1. This indicates that the proposed correction method provides a nearly constant shift over the pre-correction UD data (see Eqn. (1)). This also explains why the correlation values were very high, ranging from 0.93-0.98 for all five parameters.

3.3 Observations from "Animal-specific" CFD simulations

It is also easy to see, from Fig. 3 (also the largest RMSE in Table 1), that there were large discrepancies among velocity waveforms corresponding to Section 3 of Subject D. In order to obtain values that could be used to arbitrate these disagreements, we performed "animal-specific" computational fluid dynamic (CFD) simulations on this animal using both MRA and UD blood waveforms.

These simulations provided "idealized" velocity waveforms for each of the cross-sections from subject D based on the physics of blood flow (*i.e.* 3D time-resolved Navier-Stokes Equation [Eqns. 2 and 3]). We would thus expect that the true velocity waveform should lie in the vicinity of the CFD-calculated velocity waveforms in each of the velocity waveform plots (Fig. 4). The prescribed flow rate waveforms based on the UD and MRA measurements are labeled as D-0 in Fig. 4. Visually, in both Sections 1 and 2 (Fig. 4), the CFD-calculated velocity waveforms were in good agreements with both the UD and MRA velocity measurements. However, the UD velocity measurements in Section 3 were significantly higher (approximately 60%) than both the MRA-measured waveforms and those predicted by the CFD simulations.

In order to calculate spatial velocity gradient at the measurement locations (*i.e.* $\sqrt{\left(\frac{\partial u_x}{\partial x}\right)^2+\left(\frac{\partial u_y}{\partial y}\right)^2+\left(\frac{\partial u_z}{\partial z}\right)^2}$ where u_x, u_y and u_z are three components of the CFD-simulated velocity vector), one sample volume ($1 \times 1 \times 1$ mm^3) comparable to the size of UD sample volume was selected for each of three measurement sites (D-1, D-2 and D-3). Each sample volume centered at the centerline of respective measurement cross-sectional plane. The averaged and maximum spatial CFD-simulated velocity gradients over the corresponding sample volume are illustrated in Fig. 5 for a cardiac cycle. It is easy to see, from Fig. 5, that spatial velocity gradients at D-3 are higher than these estimated at either D-1 and D-2. The sharp spatial velocity gradients at D-3 are likely due to the fact that the measurement site D-3 was close to the velocity jet (see the horizontal arrow in Fig. 4).

4. Discussion

Without applying the proposed spectral broadening correction method, UD could significantly overestimate (see Table 3) all three parameters (PSV, MV EDV) by 26.6 cm/s (or 29.0%), 13.4 cm/s (or 28.2%) and 7.2 cm/s (or 25.2%), respectively. The overestimation of PSV by the pre-correction UD data could be further confirmed by comparing to the MRA measurements as shown in Table 2. More specifically, as compared to the MRA measurements, the pre-correction UD data would have significantly overestimated the peak systolic velocity values by 29.2 cm/s. This observation is consistent with those of other studies, where overestimations by UD have been as high as 47% (Wendt *et al.*, 1992; Hoskins, 1996). The potential for this inaccuracy is illustrated well in one of the waveforms investigated. At cross-section 3 in subject D (Figs. 3 and 4), UD overestimated the velocities

by as much as 60% compared to both the PC-VIPR MRA and the velocities predicted by "animal-specific" CFD simulations.

In Fig. 5, we found stronger spatial velocity gradients near the cross-section D-3 as compared to the other two measurement sites (D-1 and D-2). Although we observed that the complexity of the flow streamlines (*i.e.* the presence of helical flow and recirculation zones) in and around the bifurcation aneurysm increases significantly compared to the upstream parent artery and further downstream away from the bifurcation aneurysm (Fig. 4), no turbulence was identified. Thus, we stipulate that the presence of strong velocity gradients such as this causes significant spectral broadening (Campbell *et al.*, 1989) at the cross-section D-3, though the actual cause of this discrepancy could be multi-factorial and is unknown. It is likely that the simple correction for V_{corr} is inadequate for these extreme conditions, leading to ultrasound Doppler derived velocities that significantly overestimated (60%) the true velocity for Section 3 in Subject D (Hoskins, 2002).

It is also interesting to note that there were only weak correlations for the PI (r=0.35 and 0.25 for the pre- and post-correction UD data, respectively) and the RI (r=0.23 and 0.14 for the pre- and post-correction UD data, respectively) determined from the UD and PC-VIPR MRA measured velocity waveforms. Since the PI and RI have been used for various clinical applications to assess the resistance of blood flow (Petersen *et al.*, 1997; Pinggera *et al.*, 2008), further investigations are warranted to delineate conditions for which such parameters lead to erroneous results.

Doppler ultrasound is the method of choice for evaluation of blood flow in many clinical applications *e.g.* carotid artery evaluation. Its advantages over other techniques include its portability, real-time imaging capability, high temporal resolution and, instant information on peak velocities under various physiologic conditions. Improvements in ultrasound flow imaging are ongoing (Hoskins, 2002; Ivancevich *et al.*, 2008; Haworth *et al.*, 2008). Any assessment of the potential clinical utility of these and other new developments in velocity assessments using ultrasound requires that they be evaluated and compared *in vivo* against state of the art PC-MRA techniques (Gu *et al.*, 2005; Wigstrom *et al.*, 1996; Markl *et al.*, 2003; Johnson *et al.*, 2008) or other gold standards. To our knowledge, this is the first study to compare *in vivo* ultrasound Doppler measurements with results from a 4D accelerated PC-MRA technique, in this case the PC-VIPR approach.

As proposed by Steinman and colleagues, the incorporation of ultrasound and PC-MRA data that combine "subject specific" geometry information and velocity waveforms into computer flow models for simulation of hemodynamics (Steinman *et al.*, 2003) allows calculation of expected/idealized ranges of flow velocities. We recognize that neither CFD-calculated (Roache, 1997) or 4D PC-MRA measured flow is not sufficient to serve as the gold standard to validate the UD measurements. However, they do, in our opinion, serve as tools for performing valid comparisons of measured flow parameters. This is important, especially for *in vivo* flow determinations where validation of the accuracy of techniques is incomplete. Our work explored the use of this approach.

We also demonstrated that corrections for spectral broadening are needed in order to obtain reliable ultrasound Doppler measurements (see Tables 2 and 3), especially for peak systolic velocity measurements. While the proposed simple correction scheme could be easily used in a clinical setting since all parameters used in this study are readily available to clinicians, broad application of the ultrasound Doppler approach may be more limited since our measurements included only superficial arteries studied using a high-frequency linear array transducer. For this preliminary study, we also limited our effort to investigate the correlations between MRA and ultrasound velocity parameters and waveforms to only a

small number of animals. In the future we will extend our effort to obtain volumetric flow information (*e.g.* flow rate) using 3-D ultrasound flow imaging to compare these to measurements made by the PC-VIPR MRA technique. Further studies are needed to validate Doppler ultrasound use with other transducers and other scanning conditions.

Besides the small number of animals (14 waveforms in 4 subjects), another limitation of this study is that the locations of flow measurements were manually aligned using anatomical features. The accuracy of such alignment was not verified in this study. In future work, fiducial markers both visible under Ultrasound and MR will be implanted for more precise and accurate alignment.

5. Conclusions

After application of a scheme for correcting for Doppler spectral broadening, the agreement between velocity waveforms and peak systolic velocities (PSV) obtained from UD and those derived from 3D-PC-MRA velocity was very good, with correlation values of 0.89 and 0.83 for waveforms and peak systolic velocities, respectively. The potential clinical importance of these techniques warrants further study.

Acknowledgments

We are grateful to colleagues at the University of Wisconsin (especially Ms. Kari Pulfer, Ms. Kelly Hellenbrand, Dr. Carol Mitchell PhD and Dr. Mark Kliewer MD) for their assistance in equipment access and data acquisition during animal experiments. We also want to thank Ted Fisher for supplying Ultrasound beam data and anonymous reviewers for their constructive critiques that have helped us to significantly improve our manuscript. This work is, in part, supported by a research grant (R01HL072260) from the US National Institute of Health.

Appendix A: Correction for Intrinsic Spectral Broadening and calibration

The Doppler frequency shift f_d from a unidirectional flow (with a velocity of V) can be estimated as follows:

$$f_d = \frac{2f_0}{c} V \cos \quad \theta \tag{A1}$$

where θ is the Doppler angle, f_0 is the center frequency of the Ultrasound and c is the speed of sound in the medium of propagation.

Effects of Doppler bandwidth B_d are well understood in the literature with major contributions from Newhouse and colleagues(Newhouse *et al.*, 1987; Newhouse *et al.*, 1994). It can be computed using,

$$B_d = \frac{2f_0}{c} \frac{W}{F} V \mathrm{Sin} \quad \theta \tag{A2}$$

where W is the active aperture width and F is the focal length. Tortoli et al. (Tortoli *et al.*, 1995) combined Eqns. (A1-A2) together by assuming the maximum Doppler frequency due to the intrinsic spectral broadening, (ISB) effect is $f_d + B_d / 2$. They showed that the rate of overestimation α can be calculated as follows(Tortoli *et al.*, 1995; Winkler and Wu, 1995),

$$\alpha = \frac{V_{\max}}{V} = 1 + \frac{W}{2F} \tan \quad \theta \tag{A3}$$

where $V_{\max}$ is the estimated velocity based on the maximum Doppler frequency and V is the true unidirectional velocity.

Eqn. (A3) has been used to correct for the ISB effect by others(Winkler and Wu, 1995). However, Eqn. (A3) is only theoretically valid for Doppler angles that are nearly 90 degree (Censor *et al.*, 1988). To avoid over-corrections that we and others (Winkler and Wu, 1995) have observed for intermediate Doppler angles (31-72°), we empirically limited the maximum correction ΔV is less than half of the width of the actual Doppler velocity spectrogram. The width of the actual Doppler velocity spectrogram is defined by the difference between the inner velocity V_{inner} and the outer velocity V_{outer} as shown in Fig. 2(a). Therefore, the corrected velocity V_{corr} reads,

$$V_{corr}=\max\left(V_{outer}-\frac{V_{outer}}{\alpha},\frac{V_{outer}+V_{inner}}{2}\right) \quad \text{(A4)}$$

where max(*A, B*) is the larger value between *A* and *B*.

The linear array transducer (VFX 13-5, Siemens Healthcare [USA] Inc., Mountain View, CA) used in this study is a 192-element high frequency (5-13 MHz) ultrasound transducer. In the Doppler mode, for the sample volume chosen by the operator, the transmitted ultrasound beam is automatically focused at the nearest of possible foci with respect to the center of the sample volume. We chose the depth corresponding to the center of the sample volume to approximate the focal depth *F*.

Also, this linear array transducer is an f/1.33 transducer. Thus, the corresponding array aperture width W initially increases with the sample volume depth until reaching the maximum active number of elements (*i.e.* 32 elements).

The ultrasound transducer was calibrated using a flow phantom (Gammex 1430GS, Gammex, Middleton, WI) by an Ultrasound engineer (JJ). The flow phantom contains a 4-mm diameter tube mimicking a blood vessel embedded in a tissue-mimicking background and a microprocessor-based flow controller producing accurate, steady flow (1.0 to 10 ml/sec with less than ± 1.5% error) and highly reproducible pusatile waveforms. Only constant flow was used for the calibration based on Eqn. (A4). The velocity measurements were performed at a section of the tube parallel to the scanning surface, with a Doppler angle of 72 degrees and a sample volume with a gate size of 2-mm. The outer and inner velocities were first noted on the angle-corrected spectral waveforms and then were calculated based on Eqn. (A4) to compare with known velocity values in the phantom. A conversion curve provided by the manufacture was used to convert volume flow rates to peak velocities in the vessel. The ultrasound scanner performed well in this difficult scanning condition as demonstrated in Figure A1. The mean percent error (one standard deviation/mean velocity; 1.1-6.8%) was 4.8%.

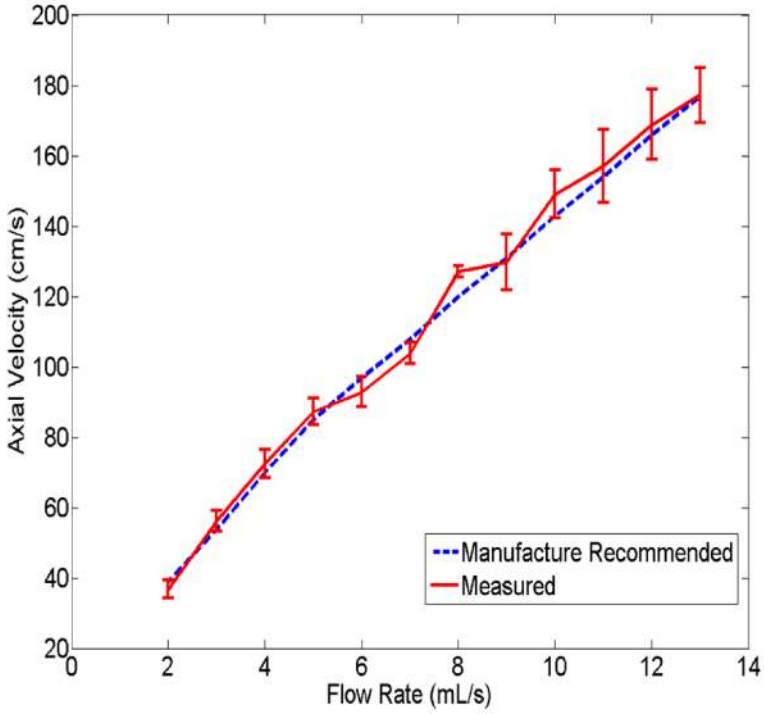

Figure A1.
A plot of Ultrasound Doppler velocity measurements (solid line) and manufacture provided conversion curve (dashed line) under various steady flow rates ranging from 2 to 13 5 ml/s. The error bar represents one standard deviation of measurement errors.

A List of Abbreviations

CCA	Common Carotid Artery
BA	Bifurcation Aneurysm
CFD	Computational Fluid Dynamics
DSA	digital subtraction angiography
EDV	End Diastolic Velocity
ISB	Intrinsic Spectral Broadening
MV	Mean Velocity
MRA	Magnetic Resonance Angiography
PC-VIPR	Phase Contrast Vastly undersampled Isotropic Projection Reconstruction
PC-MRA	Phase Contrast Magnetic Resonance Angiography
PSV	Peak Systolic Velocity
RMSE	Root Mean Squared Error
SA	Side-wall Aneurysm
SD	Standard Deviation
UD	Ultrasound Doppler

WSS Wall Shear Stress

References

Allan, PLP. Clinical Doppler ultrasound. Churchill Livingstone/Elsevier; Oxford: 2006.

Bland JM, Altman DG. Statistical methods for assessing agreement between two methods of clinical measurement. Lancet. 1986; 1:307–10. [PubMed: 2868172]

Campbell JD, Hutchison KJ, Karpinski E. Variation of Doppler ultrasound spectral width in the post-stenotic velocity field. Ultrasound Med Biol. 1989; 15:611–9. [PubMed: 2683288]

Censor D, Newhouse VL, Vontz T, Ortega HV. Theory of ultrasound Doppler-spectra velocimetry for arbitrary beam and flow configurations. IEEE Trans Biomed Eng. 1988; 35:740–51. [PubMed: 3169826]

Douville Y, Johnston KW, Kassam M. Determination of the hemodynamic factors which influence the carotid Doppler spectral broadening. Ultrasound Med Biol. 1985; 11:417–23. [PubMed: 2931873]

Dyverfeldt P, Kvitting JP, Sigfridsson A, Engvall J, Bolger AF, Ebbers T. Assessment of fluctuating velocities in disturbed cardiovascular blood flow: in vivo feasibility of generalized phase-contrast MRI. J Magn Reson Imaging. 2008; 28:655–63. [PubMed: 18777557]

Eicke BM, Kremkau FW, Hinson H, Tegeler CH. Peak velocity overestimation and linear-array spectral Doppler. J Neuroimaging. 1995; 5:115–21. [PubMed: 7718938]

Evans AJ, Iwai F, Grist TA, Sostman HD, Hedlund LW, Spritzer CE, Negro-Vilar R, Beam CA, Pelc NJ. Magnetic resonance imaging of blood flow with a phase subtraction technique. In vitro and in vivo validation. Invest Radiol. 1993; 28:109–15. [PubMed: 8444566]

Faccenda F, Rubba P, Gnasso A, Pauciullo P, Postiglione A, Cortese C, Mancini M. Noninvasive ultrasound evaluation of pressure gradients in aortic root of homozygotes for familial hypercholesterolemia. Arteriosclerosis. 1990; 10:710–3. [PubMed: 2206114]

Frayne R, Steinman DA, Ethier CR, Rutt BK. Accuracy of MR phase contrast velocity measurements for unsteady flow. J Magn Reson Imaging. 1995; 5:428–31. [PubMed: 7549205]

Fuster, V. Hurst's the heart. McGraw-Hill Medical; New York: 2008.

German WJ, Black SP. Cervical ligation for internal carotid aneurysms. An extended follow-up. J Neurosurg. 1965; 23:572–7. [PubMed: 5861140]

Gill RW. Measurement of blood flow by ultrasound: accuracy and sources of error. Ultrasound Med Biol. 1985; 11:625–41. [PubMed: 2931884]

Gross CM, Kramer J, Weingartner O, Uhlich F, Luft FC, Waigand J, Dietz R. Determination of renal arterial stenosis severity: comparison of pressure gradient and vessel diameter. Radiology. 2001; 220:751–6. [PubMed: 11526278]

Gu T, Korosec FR, Block WF, Fain SB, Turk Q, Lum D, Zhou Y, Grist TM, Haughton V, Mistretta CA. PC VIPR: a high-speed 3D phase-contrast method for flow quantification and high-resolution angiography. AJNR Am J Neuroradiol. 2005; 26:743–9. [PubMed: 15814915]

Haworth KJ, Fowlkes JB, Carson PL, Kripfgans OD. Towards aberration correction of transcranial ultrasound using acoustic droplet vaporization. Ultrasound Med Biol. 2008; 34:435–45. [PubMed: 17935872]

Holen J, Waag RC, Gramiak R. Doppler ultrasound in aortic stenosis: in vitro studies of pressure gradient determination. Ultrasound Med Biol. 1987; 13:321–8. [PubMed: 3303589]

Hoppe M, Heverhagen JT, Froelich JJ, Kunisch-Hoppe M, Klose KJ, Wagner HJ. Correlation of flow velocity measurements by magnetic resonance phase contrast imaging and intravascular Doppler ultrasound. Invest Radiol. 1998; 33:427–32. [PubMed: 9704280]

Hoskins PR. Measurement of arterial blood flow by Doppler ultrasound. Clin Phys Physiol Meas. 1990; 11:1–26. [PubMed: 2182271]

Hoskins PR. Accuracy of maximum velocity estimates made using Doppler ultrasound systems. Br J Radiol. 1996; 69:172–7. [PubMed: 8785647]

Hoskins PR. Ultrasound techniques for measurement of blood flow and tissue motion. Biorheology. 2002; 39:451–9. [PubMed: 12122266]

Hughes PE, How TV. Quantitative measurement of wall shear rate by pulsed Doppler ultrasound. J Med Eng Technol. 1993; 17:58–64. [PubMed: 8366509]

Ivancevich NM, Pinton GF, Nicoletto HA, Bennett E, Laskowitz DT, Smith SW. Real-time 3-D contrast-enhanced transcranial ultrasound and aberration correction. Ultrasound Med Biol. 2008; 34:1387–95. [PubMed: 18395321]

Jiang J, Strother C. Computational fluid dynamics simulations of intracranial aneurysms at varying heart rates: a "patient-specific" study. J Biomech Eng. 2009; 131:091001. [PubMed: 19725690]

Jiang Z-L, Yamaguchi H, Takahashi A, Tanabe S, Utsuyama N, Ikehara T, Hosokawa K, Tanaka H, Kinouchi Y, Miyamoto H. Blood flow velocity in the common carotid artery in humans during graded exercise on a treadmill. European Journal of Applied Physiology and Occupational Physiology. 1995; 70:234–9. [PubMed: 7607198]

Jin S, Oshinski J, Giddens DP. Effects of Wall Motion and Compliance on Flow Patterns in the Ascending Aorta. Journal of Biomechanical Engineering. 2003; 125:347–54. [PubMed: 12929239]

Johnson KM, Lum DP, Turski PA, Block WF, Mistretta CA, Wieben O. Improved 3D phase contrast MRI with off-resonance corrected dual echo VIPR. Magn Reson Med. 2008; 60:1329–36. [PubMed: 19025882]

Kohler U, Marshall I, Robertson MB, Long Q, Xu XY, Hoskins PR. MRI measurement of wall shear stress vectors in bifurcation models and comparison with CFD predictions. J Magn Reson Imaging. 2001; 14:563–73. [PubMed: 11747008]

Lee VS, Spritzer CE, Carroll BA, Pool LG, Bernstein MA, Heinle SK, MacFall JR. Flow quantification using fast cine phase-contrast MR imaging, conventional cine phase-contrast MR imaging, and Doppler sonography: in vitro and in vivo validation. Am. J. Roentgenol. 1997; 169:1125–31. [PubMed: 9308476]

Lotz J, Meier C, Leppert A, Galanski M. Cardiovascular Flow Measurement with Phase-Contrast MR Imaging: Basic Facts and Implementation. Radiographics. 2002; 22:651–71. [PubMed: 12006694]

Maguire, S.; Graves, MJ.; Markenroth, K.; Abolmaali, ND. ISMRM. 2006. Multi-centre in vivo Evaluation of MR Phase Contrast Flow Measurements.

Markl M, Chan FP, Alley MT, Wedding KL, Draney MT, Elkins CJ, Parker DW, Wicker R, Taylor CA, Herfkens RJ, Pelc NJ. Time-resolved three-dimensional phase-contrast MRI. J Magn Reson Imaging. 2003; 17:499–506. [PubMed: 12655592]

Nett, EJ.; Johnson, KM.; Landgraf, BR.; Wieben, O. Platform for Comprehensive Hemodynamic Analysis of 4D PC MRI Data; The 17th Scientific Meeting of International Society for Magnetic Resonance in Medicine; Hawaii. 2009;

Newhouse VL, Censor D, Vontz T, Cisneros JA, Goldberg BB. Ultrasound Doppler probing of flows transverse with respect to beam axis. IEEE Trans Biomed Eng. 1987; 34:779–89. [PubMed: 3679261]

Newhouse VL, Faure P, Cathignol D, Chapelon J-Y. The transverse Doppler spectrum for focused transducers with rectangular apertures. The Journal of the Acoustical Society of America. 1994; 95:2091–8.

Petersen LJ, Petersen JR, Talleruphuus U, Ladefoged SD, Mehlsen J, Jensen HA. The pulsatility index and the resistive index in renal arteries. Associations with long-term progression in chronic renal failure. Nephrol Dial Transplant. 1997; 12:1376–80. [PubMed: 9249772]

Pinggera GM, Mitterberger M, Bartsch G, Strasser H, Gradl J, Aigner F, Pallwein L, Frauscher F. Assessment of the intratesticular resistive index by colour Doppler ultrasonography measurements as a predictor of spermatogenesis. BJU Int. 2008; 101:722–6. [PubMed: 18190642]

Rayz VL, Boussel L, Acevedo-Bolton G, Martin AJ, Young WL, Lawton MT, Higashida R, Saloner D. Numerical simulations of flow in cerebral aneurysms: comparison of CFD results and in vivo MRI measurements. J Biomech Eng. 2008; 130:051011. [PubMed: 19045518]

Roache PJ. Quantification of uncertainty in computational fluid dynamics. Annual Review of Fluid Mechanics. 1997; 29:123–60.

Seitz J, Strotzer M, Wild T, Nitz WR, Volk M, Lenhart M, Feuerbach S. Quantification of blood flow in the carotid arteries: comparison of Doppler ultrasound and three different phase-contrast magnetic resonance imaging sequences. Invest Radiol. 2001a; 36:642–7. [PubMed: 11606841]

Seitz J, Strotzer M, Wild T, Nitz WR, Volk M, Lenhart M, Feuerbach S. Quantification of blood flow in the carotid arteries: comparison of Doppler ultrasound and three different phase-contrast magnetic resonance imaging sequences. Invest Radiol. 2001b; 36:642–7. [PubMed: 11606841]

Stadlbauer A, van der Riet W, Globits S, Crelier G, Salomonowitz E. Accelerated phase-contrast MR imaging: comparison of k-t BLAST with SENSE and Doppler ultrasound for velocity and flow measurements in the aorta. J Magn Reson Imaging. 2009; 29:817–24. [PubMed: 19306404]

Steiger HJ, Poll A, Liepsch D, Reulen HJ. Basic flow structure in saccular aneurysms: a flow visualization study. Heart Vessels. 1987; 3:55–65. [PubMed: 3500943]

Steinman DA, Milner JS, Norley CJ, Lownie SP, Holdsworth DW. Image-based computational simulation of flow dynamics in a giant intracranial aneurysm. AJNR Am J Neuroradiol. 2003; 24:559–66. [PubMed: 12695182]

Strother CM, Graves VB, Rappe A. Aneurysm hemodynamics: an experimental study. AJNR Am J Neuroradiol. 1992; 13:1089–95. [PubMed: 1636518]

Tortoli P, Guidi G, Newhouse VL. Improved blood velocity estimation using the maximum Doppler frequency. Ultrasound Med Biol. 1995; 21:527–32. [PubMed: 7571145]

Turk AS, Aagaard-Kienitz B, Niemann D, Consigny D, Rappe A, Grinde J, Strother CM. Natural history of the canine vein pouch aneurysm model. AJNR Am J Neuroradiol. 2007; 28:531–2. [PubMed: 17353330]

Valencia AA, Guzman AM, Finol EA, Amon CH. Blood flow dynamics in saccular aneurysm models of the basilar artery. J Biomech Eng. 2006; 128:516–26. [PubMed: 16813443]

Wendt RE 3rd, Rokey R, Wong WF, Marks A. Magnetic resonance velocity measurements in small arteries. Comparison with Doppler ultrasonic measurements in the aortas of normal rabbits. Invest Radiol. 1992; 27:499–503. [PubMed: 1644547]

Wigstrom L, Sjoqvist L, Wranne B. Temporally resolved 3D phase-contrast imaging. Magn Reson Med. 1996; 36:800–3. [PubMed: 8916033]

Winkler AJ, Wu J. Correction of intrinsic spectral broadening errors in Doppler peak velocity measurements made with phased sector and linear array transducers. Ultrasound Med Biol. 1995; 21:1029–35. [PubMed: 8553497]

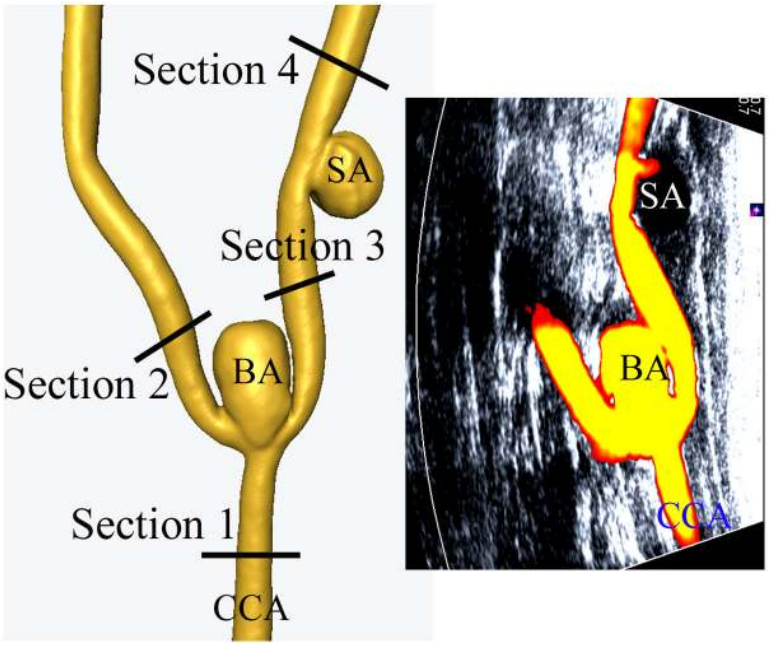

Figure 1.
A bifurcation aneurysm (BA) and a side-wall aneurysm (SA) in a canine model. The left image shows the reconstructed geometry based on 3D digital subtraction angiography (DSA), while the right image is a matched power Doppler image overlaid onto a B-mode Ultrasound image. CCA in both images stands for the common carotid artery. Sections 1-4 are approximately four planes where UD measurements were made in this animal. The 3D DSA data were obtained using a clinical angiographic C-arm device (Axiom Artis dBA, Siemens Medical System Inc., Forchheim, Germany). Since the ultrasound scanning plane was set to visualize the bifurcation aneurysm, the side-wall aneurysm is not seen well in the right image.

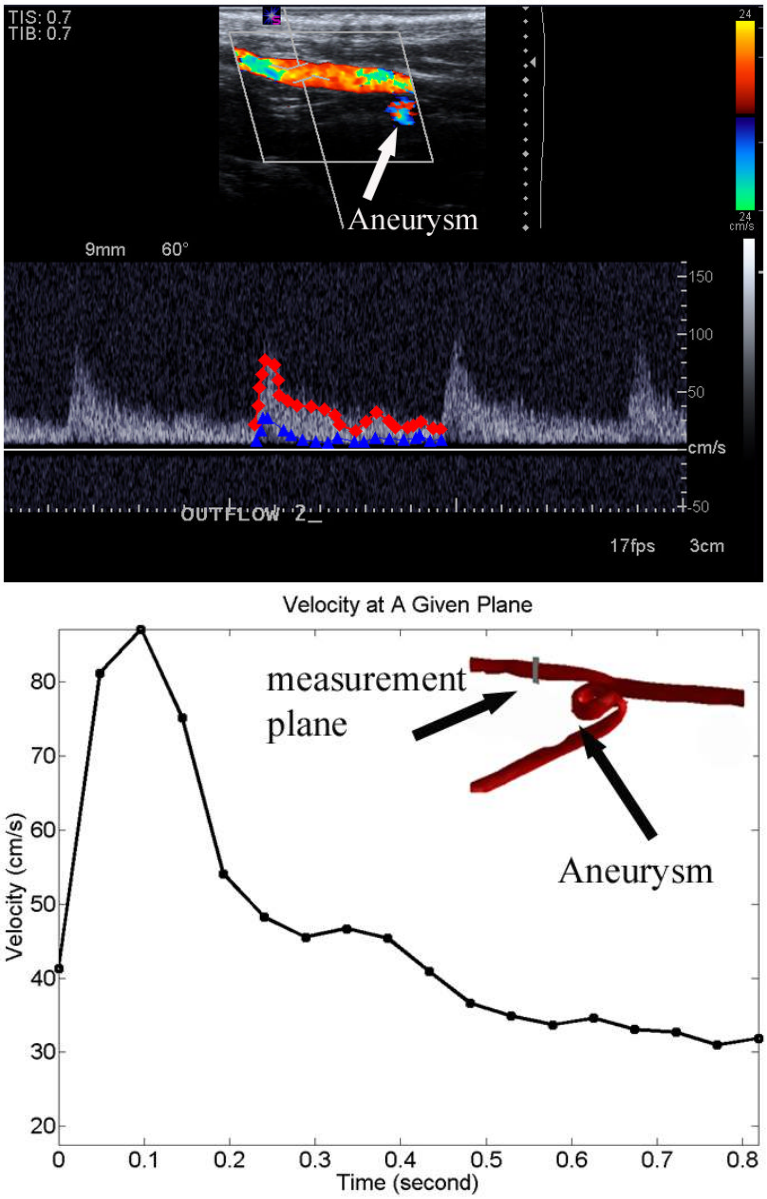

Figure 2.

Schematic illustrations of off-line processing of velocity waveforms: (a) UD Velocity Spectrogram and (b) 4D/3D PC-VIPR MRA. In (a), the red line with diamond markers and the blue line with triangle markers are the outer and inner velocity waveforms, respectively. Both lines are used in Eqn. (1). In (b), a MRA velocity waveform obtained from a matched imaging plane (slice thickness 0.8-mm) is displayed.

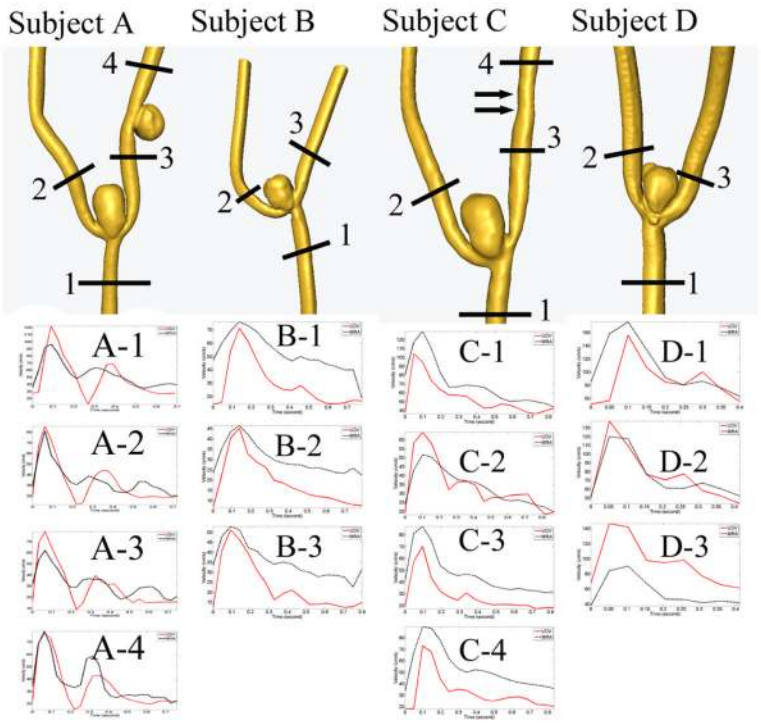

Figure 3.

Plots of velocity waveforms among Subjects A-D. Velocity measurements were performed at either four or three cross-sectional planes for each subject. The top row shows geometries and labeled cross-sectional planes, while the bottom four rows show respective velocity waveforms. For instance, “A-1” stands for the Section 1 in Subject A. The labels “UDV” and “MRA” refers to velocity data from UD (red) and MRA (black) measurements. Double horizontal arrows in Subject C point to the location of the side-wall aneurysm that was largely occluded due to spontaneous thrombosis.

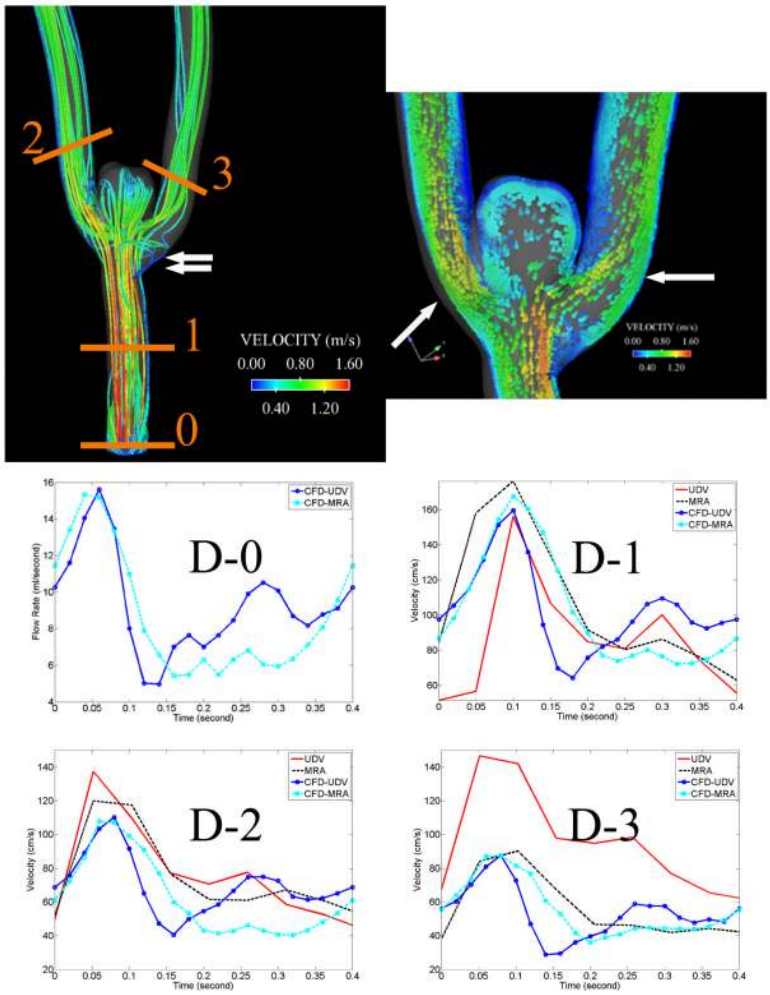

Figure 4.

An image showing streamlines (*i.e.* lines of tangent to instantaneous velocity vectors) of CFD simulated velocity vectors at peak systole in Subject D is displayed in the top left, while a three-dimensional velocity vector plot at a cutting plane of the same subject is shown in the top right. The input flow rate waveforms prescribed at the inlet (D-0) are shown in the middle left. The rest graphs in the bottom two rows illustrate CFD-simulated velocity waveforms (dashed cyan [MRA] and solid blue [UD] lines), UD-measured (solid red line), and MRA-measured (dashed black line) velocity waveforms at three different cross-sectional planes (D-1, D-2 and D-3) of this subject. The CFD-simulated velocities from which streamlines were derived were based on UD flow rates. The inclined and horizontal arrows in the 3D velocity vector plot (top right) point to velocity jets nearly the measurement sections D-2 and D-3, respectively. The double arrows in the streamline plot (top left) point to the disturbed low velocity region proximal to D-3.

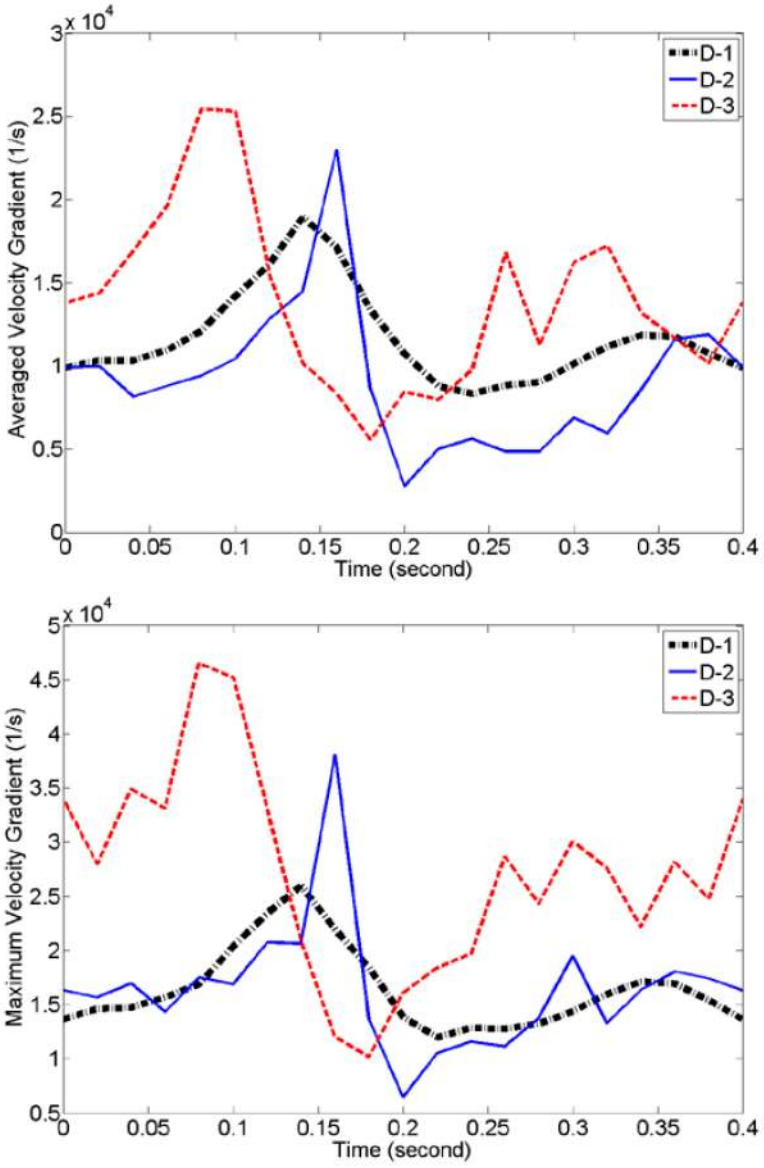

Figure 5.
Plot of (a) averaged and (b) maximum spatial velocity gradients over the pre-selected sample volumes ($1 \times 1 \times 1$ mm^3) for a cardiac cycle. The CFD-simulated velocities from which spatial gradients were derived were based on UD flow rates (see Fig. 4).

Table 1

Calculated RMSE values (cm/s) between the UD and the PC-VIPR MRA velocity waveforms before and after the correction method is applied among Subjects A-D. RMSE values are also normalized by the corresponding "post-correction" mean velocity values and included in the parentheses. Normalized RMSE values are unit-less quantities.

	Subject	Section 1	Section 2	Section 3	Section 4
"Post-Correction"	A	18.3 (0.378)	10.1 (0.311)	10.9 (0.371)	10.8 (0.322)
	B	24.9 (0.858)	12.0 (0.627)	13.2 (0.466)	N/A
	C	19.7 (0.364)	6.2 (0.181)	19.0 (0.678)	22.6 (0.700)
	D	37.7 (0.443)	10.3 (0.136)	41.4 (0.438)	N/A
"Pre-Correction"	A	26.6 (0.548)	14.9 (0.366)	14.4 (0.489)	15.5 (0.461)
	B	19.6 (0.675)	10.3 (0.540)	10.8 (0.574)	N/A
	C	10.7 (0.197)	14.1 (0.411)	10.6 (0.377)	14.0 (0.434)
	D	29.5 (0.346)	35.8 (0.476)	63.6 (0.673)	N/A

Phys Med Biol. Author manuscript; available in PMC 2012 June 28.

Table 2

Statistical comparison between the UD and the PC-VIPR MRA methods for 5 velocity parameters (PSV, MV, EDV, PI and RI). Note that, in linear regression analysis, ultrasound Doppler velocity parameters are in the X-axis, while MRA velocity parameters are in the Y-axis. As compared to a quantity estimated by the PC-VIPR technique, positive and negative mean differences calculated by the Bland-Altman method indicate underestimation and overestimation of the quantity by the UD technique, respectively.

(a) Post-correction UD vs. PC-VIPR MRA

		PSV	MV	EDV	PI (unitless)	RI (unitless)
Absolute Diff (cm/s) mean ± standard deviation		16.4 ± 14.1	12.7 ± 10.4	8.1 ± 7.3	0.49 ± 0.34	0.09 ± 0.08
Bland-Altman	Mean Diff (cm/s)	−2.6	6.9	4.4	−0.47	−0.08
	l.lim ~ u.lim (cm/s)	−56.5 ~ 25.0	−38.4 ~ 23.0	−16.0 ~ 25.6	−1.18 ~ 0.08	−0.31 ~ 0.07
Spearman's Correlation	r	0.83	0.76	0.81	0.25	0.14
	P-value	<0.001	0.002	<0.001	0.39	0.64
Linear Regression	Slope	0.78	0.67	0.65	0.24	0.12
	Y-Intercept (cm/s)	17.8	21.5	13.8	0.75	0.56

(b)Pre-correction UD vs. PC-VIPR MRA

		PSV	MV	EDV	PI (unitless)	RI (unitless)
Absolute Diff (cm/s) (mean ± standard deviation)		30.7 ± 26.4	13.4 ± 14.4	8.3 ± 9.8	0.49 ± 0.33	0.10 ± 0.09
Bland-Altman	Mean Diff (cm/s)	−29.2	−6.5	−2.7	−0.47	−0.08
	l.lim ~ u.lim (cm/s)	−89.5 ~ 5.1	−59.4 ~ 9.9	−39.6 ~ 13.7	−1.13 ~ 0.07	−0.31 ~ 0.07
Spearman's Correlation	r	0.81	0.85	0.78	0.35	0.23
	P-value	<0.001	<0.001	<0.001	0.21	0.43
Linear Regression	Slope	0.57	0.53	0.52	0.29	0.17
	Y-Intercept (cm/s)	21.2	20.5	13.6	0.68	0.52

Table 3

Statistical comparison between the pre- and post-correction UD velocity parameters (PSV, MV, EDV, PI and RI). Note that, in linear regression analysis, the pre-correction UD velocity parameters are in the X-axis, while the post-correction UD velocity parameters are in the Y-axis. As compared to a quantity estimated by the post-correction UD data, positive and negative mean differences calculated by the Bland-Altman method indicate overestimation and underestimation of the quantity by the pre-correction UD data, respectively.

		PSV	MV	EDV	PI (unitless)	RI (unitless)
Absolute Diff (cm/s) mean ± standard deviation		26.6 ± 15.9	13.4 ± 9.3	7.2 ± 6.6	0.09 ± 0.08	0.02 ± 0.02
Bland-Altman	Mean Diff (cm/s)	26.6	13.4	7.2	0.002	0.006
	l.lim ~ u.lim (cm/s)	6.0 ~ 61.0	−3.1 ~ 36.8	1.0 ~ 27.8	−0.21 ~ 0.28	−0.035 ~ 0.045
Spearman's Correlation	r	0.94	0.95	0.98	0.96	0.93
	P-value	<0.001	<0.001	<0.001	<0.001	<0.001
Linear Regression	Slope	0.70	0.72	0.73	0.94	0.95
	Y-Intercept (cm/s)	8.2	2.3	2.1	0.09	0.03